

# POLARIZATION MEASUREMENT AND MODELING OF VISIBLE SYNCHROTRON RADIATION AT SPEAR3\*

C. L. Li<sup>†</sup>, East China University of Science and Technology, Shanghai, China

J. Corbett, SLAC National Accelerator Laboratory, Menlo Park, USA

Y. H. Xu, Donghua University, Shanghai, China

W.J. Zhang, East China University of Science and Technology, Shanghai, China  
and the University of Saskatchewan, Saskatoon, Canada

## Abstract

Synchrotron radiation from dipole magnets is linearly polarized in the plane of acceleration and evolves toward circular polarization with increasing vertical observation angle. The intensity of the x-y field components can be modeled with Schwinger's theory for the angular-spectral power distribution. Combined with Fresnel's laws for reflection at a mirror surface, it is possible to model field polarization of visible SR light in the laboratory. The polarization can also be measured with a polarizer and quarter wave plate to yield Stokes' parameters  $S_0$ - $S_3$ . In this paper we present measurements and modeling of the visible SPEAR3 SR beam in terms of Stokes' parameters and plot on the results on the Poincaré sphere.

## INTRODUCTION

Synchrotron radiation (SR) has the unique property of a high degree of field polarization. The SR beam from a dipole magnet, for instance, is linearly polarized in the transverse acceleration plane, and changes to elliptical and finally circular polarization as the vertical observation angle increases [1]. Polarized SR in the UV or X-ray regime is frequently used to probe structural properties of matter [2]. Visible SR, with a relatively large opening angle, provides a unique opportunity to study the SR beam polarization state.

According to Schwinger's theory for synchrotron radiation, the  $\sigma$ - and  $\pi$  mode power density distributions produced from a dipole magnet can be accurately modeled. By combining with Fresnel's equations for reflection of electromagnetic radiation at a material interface, the beam polarization at the SR source and at the optical bench can be modeled.

For this work we constructed an optical measurement system composed of a bandpass filter, field-discriminating polarizer and quarter wave plate (QWP) to characterize the beam polarization state in terms of Stokes's parameters [3,4]. The measurement system is mounted on a continuous-scan vertical stage to record the beam intensity as a function of vertical observation angle and polarizer rotation angle. Preliminary results have been presented in references [5,6]. In this paper, we extend the analysis to a Stokes' parameter representation, extract beam polarization ellipse parameters and display the results on the Poincaré sphere.

\* Work supported by US Department of Energy Contract DE-AC03-76SF00515, Office of Basic Energy Sciences and the China Scholarship Council.

<sup>†</sup> Corresponding author: chunlei520@gmail.com

## THE SPEAR3 DIAGNOSTIC BEAMLINE

As shown in Fig. 1, the unfocused visible SR beam first encounters a Rhodium-coated extraction mirror at an incidence angle of 81 degrees to the surface normal. The beam is then reflected by two near-normal Al mirrors onto the optical bench. An image of the unfocused SR beam at a distance  $\sim 16$ m from the source is seen to the right. A 'cold finger' x-ray beam stop shadows a range of  $\pm 0.6$  mrad at the accelerator midplane to protect the extraction mirror from high heat loads at 500mA electron beam current.

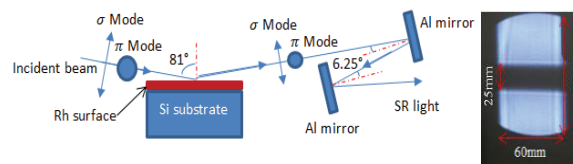


Figure 1: Schematic diagram of the visible-light SR beam transport line at SPEAR3.

Table 1: Reflection Properties of the Rh-coated Mirror

Parameters	Value
Wavelength (nm)	532
Refractive index ( $n_r$ )	2.633
Extinction index ( $k_i$ )	3.306
Reflection coefficient $r_s(\pi \text{ mode})$	0.957
Reflection coefficient $r_p(\sigma \text{ mode})$	0.508
Intensity ratio $I_p/I_s=(r_p/r_s)^2$	0.2818
$\pi$ mode phase shift $\Delta\phi_s$	-176.726°
$\sigma$ mode phase shift $\Delta\phi_p$	119.555°
Phase difference $\Delta\phi_{s-p}$	above=153.6°

The visible SR beam extraction mirror was manufactured with 600Å Rhodium deposited on a monolithic Si block [7]. As a result, the refractive index  $n_r$  and extinction index  $k_i$  exhibit 'thin film' properties as found in [8]. The corresponding reflection coefficients listed in Table 1 were calculated using Fresnel's laws [9] with a complex index of refraction  $n=n_r+ik_i$ . The grazing-incidence reflection angle in combination with the thin-film Rh mirror surface properties results in  $\sim 75\%$  power loss of the horizontal beam polarization component ( $\sigma$ -mode radiation). The normal-incidence Al mirrors have only a small effect.

Stokes' parameters for the unfocused beam were measured using the continuous-scan data acquisition system to systematically probe the vertical observation

angle and rotate the polarizer transmission axis [10,11]. A typical elevation/rotation scan contains 240360 points and requires ~8 hours to acquire.

## SCHWINGER'S EQUATIONS

Schwinger's equations can be used to calculate the vertical SR beam intensity profile as a function of radiation frequency. The single-particle intensity distribution for the  $\sigma$  and  $\pi$  polarization components from a dipole magnet can be written in compact form as [1]

$$F_{\sigma} = \left(\frac{3}{2\pi}\right)^3 \left(\frac{\omega}{2\omega_c}\right)^2 (1 + \gamma^2 \psi^2)^2 K_{\frac{2}{3}}^2 \left(\frac{\omega}{2\omega_c} (1 + \gamma^2 \psi^2)^{\frac{3}{2}}\right) \quad (1)$$

$$F_{\pi} = \left(\frac{3}{2\pi}\right)^3 \left(\frac{\omega}{2\omega_c}\right)^2 \gamma^2 \psi^2 (1 + \gamma^2 \psi^2)^2 K_{\frac{1}{3}}^2 \left(\frac{\omega}{2\omega_c} (1 + \gamma^2 \psi^2)^{\frac{3}{2}}\right) \quad (2)$$

where  $\omega = 2\pi f$  is the angular frequency of the light,  $\psi$  is the vertical observation angle,  $\gamma$  is the relativistic Lorentz factor for the radiating charges and  $\omega_c$  is the 'critical frequency' characteristic of the radiated power spectrum.  $K_{1/3}$  and  $K_{2/3}$  are modified Bessel functions. By inspection  $F_{\sigma}$  is finite at the orbit midplane and  $F_{\pi}$  has a null at the midplane where  $\gamma\psi=0$ . The functional arguments  $\omega/\omega_c$  and  $\gamma\psi$  are normalized so the equations for SR emission are valid over a range different magnetic fields and charged particle beam energies.

For visible light, it is of interest to experimentally validate these expressions in the regime where  $\omega \ll \omega_c$  by comparing with measured results. The key observation parameters for SPEAR3 are defined in Table 2.

Table 2: SPEAR3 Experiment Parameters at 3GeV

Parameter	Value
Observation wavelength	532 nm
Observation angle ( $\psi$ )	-3.5 to +3.5 mrad
Lorentz factor ( $\gamma$ )	5860.8
Crit. Energy ( $h\nu_c, \omega/\omega_c$ )	7.6keV, $3 \times 10^{-4}$

## STOKES' PARAMETERS AND THE BEAM POLARIZATION ELLIPSE

Stokes' parameters are often used to describe the polarization state of light. The four parameters  $S_0$ - $S_3$  define measurable beam intensity quantities that can be obtained using a field polarizer and a quarter waveplate (QWP) [3,4]. Stokes' parameters are valid for unpolarized light, partially polarized light and fully polarized light, in the latter case synchrotron radiation.

Mathematically, two orthogonal components for monochromatic polarized light can be represented by [4]

$$E_x = E_{ox} \cos(\omega t - kz + \delta_x) = E_{ox} e^{i(\omega t - kz + \delta_x)} \quad (3)$$

$$E_y = E_{oy} \cos(\omega t - kz + \delta_y) = E_{oy} e^{i(\omega t - kz + \delta_y)} \quad (4)$$

As shown in Fig. 2, these equations can be combined to define a 'beam polarization ellipse' by eliminating the

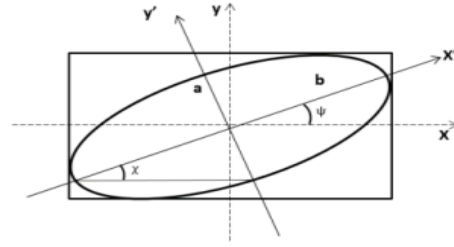


Figure 2: Typical beam polarization ellipse.

common propagation factor  $\omega t - kz$ :

$$\frac{E_x^2(t)}{E_{ox}^2} + \frac{E_y^2(t)}{E_{oy}^2} - 2 \frac{E_x(t) E_y(t)}{E_{ox} E_{oy}} \cos \delta = \sin^2 \delta \quad (5)$$

Mathematically, the electric field transmitted through a phase-shifting 'wave plate' which delays  $E_x$  by  $\varphi$  followed by a polarizer oriented at angle  $\theta$  to the x-axis can be expressed as

$$E = E_x e^{-i\varphi} \cdot \cos \theta + E_y \cdot \sin \theta. \quad (6)$$

In 1852 G.G. Stokes' demonstrated that by squaring Eq. 6 ( $E^*E$ ) and using trigonometric double-angle formulas the beam intensity can be written in terms of *measurable* quantities [3]:

$$I(\theta, \varphi) = E \cdot E^* = \frac{1}{2} [(E_{ox}^2 + E_{oy}^2) + (E_{ox}^2 - E_{oy}^2) \cos 2\theta + (2E_{ox}E_{oy} \cos \delta) \cos \varphi \sin 2\theta + (2E_{ox}E_{oy} \sin \delta) \sin \varphi \sin 2\theta] \quad (7)$$

where  $\delta = \delta_x - \delta_y$  and time averages are implied.

In terms of Stokes' parameters  $S_0$ - $S_3$ , Eq. 7 can be expressed as

$$I(\theta, \varphi) = \frac{1}{2} [S_0 + S_1 \cos 2\theta + S_2 \cos \varphi \sin 2\theta + S_3 \sin \varphi \sin 2\theta] \quad (8)$$

where

$$S_0 = I(0^\circ, 0^\circ) + I(90^\circ, 0^\circ) = E_{ox}^2 + E_{oy}^2 \quad (8a)$$

$$S_1 = I(0^\circ, 0^\circ) - I(90^\circ, 0^\circ) = E_{ox}^2 - E_{oy}^2 \quad (8b)$$

$$S_2 = I(45^\circ, 0^\circ) - I(135^\circ, 0^\circ) = 2E_{ox}E_{oy} \cos \delta \quad (8c)$$

$$S_3 = I(45^\circ, 90^\circ) - I(135^\circ, 90^\circ) = 2E_{ox}E_{oy} \sin \delta \quad (8d)$$

The beam polarization ellipse shown in Fig. 2 has a rotation angle  $\psi$  and a characteristic ellipticity angle  $\chi$  where  $\tan \chi = \pm a/b$  that can be expressed either in terms of field parameters  $\{E_{ox}, E_{oy}, \delta\}$ , or Stokes' parameters:

$$\tan 2\Psi = \frac{2E_{ox}E_{oy} \cos \delta}{E_{ox}^2 - E_{oy}^2} = \frac{S_2}{S_1} \quad (10)$$

$$\sin 2\chi = \frac{2E_{ox}E_{oy} \sin \delta}{E_{ox}^2 + E_{oy}^2} = \frac{S_3}{S_0} \quad (11)$$

The relation between Stokes' parameters and the beam polarization ellipse parameters  $\psi$  and  $\chi$  can be re-written

$$S_2 = S_1 \tan 2\Psi \quad (12)$$

$$S_3 = S_0 \sin 2\chi \quad (13)$$

For a fully-polarized beam, Stokes' parameters obey

$$S_0^2 = S_1^2 + S_2^2 + S_3^2 \quad (14)$$

Substituting Eqs. 12 and 13 into Eq. 14, we obtain

$$S_1 = S_0 \cos 2\chi \cos 2\Psi \quad (15a)$$

$$S_2 = S_0 \cos 2\chi \sin 2\Psi \quad (15b)$$

$$S_3 = S_0 \sin 2\chi \quad (15c)$$

By analogy, standard spherical coordinates  $\{r, \theta, \phi\}$  are related to the Cartesian coordinate axes  $\{x, y, z\}$  by

$$x = r \sin \theta \cos \phi \quad (16a)$$

$$y = r \sin \theta \sin \phi \quad (16b)$$

$$z = r \cos \theta \quad (16c)$$

$S_1, S_2, S_3$  in Eqs. 15 may therefore be identified with Cartesian coordinate axes provided

$$\theta = 90^\circ - 2\chi \quad \text{and} \quad \phi = 2\Psi.$$

As first demonstrated by Poincaré [4], the polarization state of light can be plotted in terms of ellipse parameters  $\psi$  and  $\chi$  on the 'Poincaré sphere' illustrated in Fig. 3. In the equatorial plane ( $S_3=0$ ) the field is linearly polarized and at the poles the field is circularly polarized. All states between the equator and the two poles represent elliptical polarization. Interestingly, nearby points on the sphere represent similar polarization states and therefore have the potential to produce interference fringes.

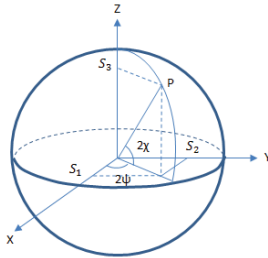


Figure 3: Poincaré sphere for field polarization.

## MEASUREMENT AND MODEL

Intensity profiles were first measured along the vertical observation axis for the  $E_{0x}^2$  and  $E_{0y}^2$  SR field components at  $\lambda=532\text{nm}$ . Stokes' parameters  $S_0$  and  $S_1$  were then calculated by substituting the data into Eqs. 8a and 8b and plotted in Figs. 4 and 5. The solid red lines are the theoretical values from Schwinger's equations taking account attenuation at the Rh-coated beam extraction mirror (Table 1) [6].

$S_2$  was measured by rotating the polarizer to  $45^\circ$  and  $135^\circ$  relative to the horizontal axis and calculating the intensity difference from Eq. 8c. The measured data is plotted in Fig. 6. The theoretical solid red curve was obtained from Eq. 8c where  $E_{ox}$  and  $E_{oy}$  are the scaled Schwinger equations and the relative phase  $\delta=153.56^\circ$  (see Table 1). To improve the model, the black curve retains Schwinger intensity profiles but introduces the *measured* phase shift at the mirror derived from Eq. 8c [6]. The natural phase

ISBN 978-3-95450-177-9

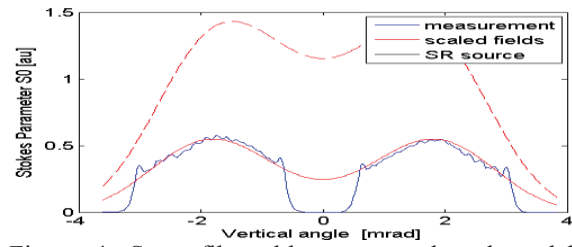


Figure 4:  $S_0$  profile - blue=measured, red=model with mirror attenuation, red-dash=SR source.

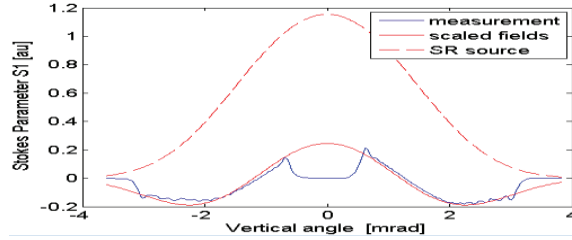


Figure 5:  $S_1$  profile - blue=measured, red=model with mirror attenuation, red-dash=SR source.

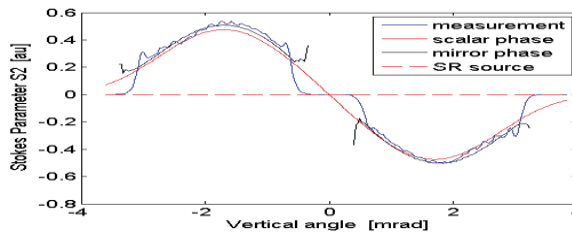


Figure 6:  $S_2$  profile - blue=measured, red=model phase shift, black=measured phase, dash=SR source.

difference at the SR source point is  $\delta=\pm 90^\circ$ .

In practice the phase shift induced by the extraction mirror evaluated along the vertical observation axis is important for modeling the beam polarization state. As seen in Fig. 7, the model for the ellipticity angle  $\chi$  is inaccurate when a fixed scalar value is used for the phase shift. If the *measured* phase profile is used in the model, the agreement between measured and modeled ellipticity angle improves significantly.

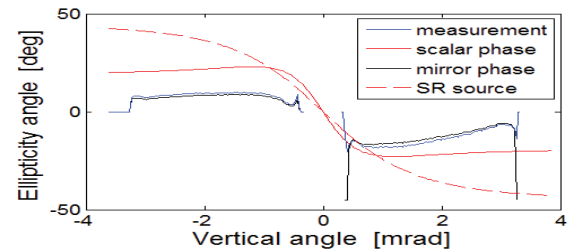


Figure 7: Profile for ellipticity angle - blue=measured, red=model phase shift, black=measured phase shift, red dash=SR source.

Stokes' parameter  $S_3$  yields the 'handedness' of helically polarized light.  $S_3$  was measured by inserting the QWP upstream of the polarizer with the fast axis oriented vertically and again setting the polarizer to  $45^\circ$  and  $135^\circ$ , respectively. Figure 8 shows the measured  $S_3$  profile (blue) and the calculated value after the Rh-mirror (solid red). The black curve is the result of using the measured

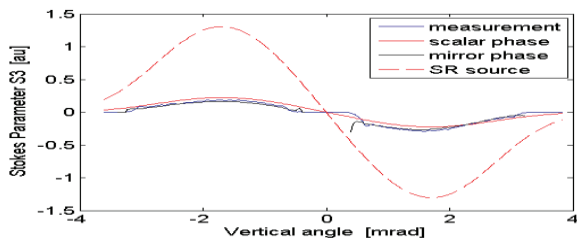


Figure 8:  $S_3$  profile - blue=measured, red=model phase shift, black=measured phase, dash=SR source.

phase profile. The red-dashed line represents  $S_3$  at the SR source. The reduction in magnitude of  $S_3$  demonstrates that the Rh extraction mirror converts helically-polarized light to much more linearly-polarized light.

Figure 9 shows the Poincaré sphere representation of the normalized beam polarization state as a function of vertical observation angle. The axes of the Poincaré sphere represent Stokes' parameters  $\{S_1, S_2, S_3\}$ . The ellipticity angle  $\chi$  corresponds to latitude and the ellipse rotation angle  $\psi$  corresponds to longitude (Fig. 3). For the SPEAR3 data, the upper half of the sphere contains the SR beam below the accelerator midplane while the lower half shows the beam above the midplane.

The blue line in Fig. 9 shows the theoretical variation in beam polarization state at the SR source – the light is linearly polarized at the midplane ( $S_3=0$ ) with increasing ellipticity and no ellipse rotation angle  $\psi$  (natural dipole SR lies entirely in the  $S_1$ - $S_3$  plane). The green line shows the measured polarization trajectory. The field is significantly more 'linearly' polarized than at the source due to the phase shift at the extraction mirror. The presence of the cold finger is evident in the data (accelerator midplane).

The red line shows the calculated polarization state after the extraction mirror when a fixed scalar value is used for phase shift at the mirror. The trajectory is slightly offset in  $2\chi$  from the measured data. When the measured phase is used in the calculation the agreement between measurement and model is good (magenta model curve on top of blue measured data).

### CONCLUSIONS

Field polarization measurements of an unfocused visible SR beam are presented and modeled using Schwinger's equations to calculate vertical elevation dependence and the Stokes' parameters to represent the polarization state. Fresnel's equations were used to simulate reflection from the Rh-coated beam pick-off mirror. The data is plotted on the Poincaré sphere to yield a compact representation of the variation in beam polarization with vertical observation angle. The close agreement between measurement and model confirms Schwinger's theory in the visible light regime ( $\omega \ll \omega_c$ ) and demonstrates the thin-film Rh-coated beam pick-off mirror has a significant influence on the extracted light.

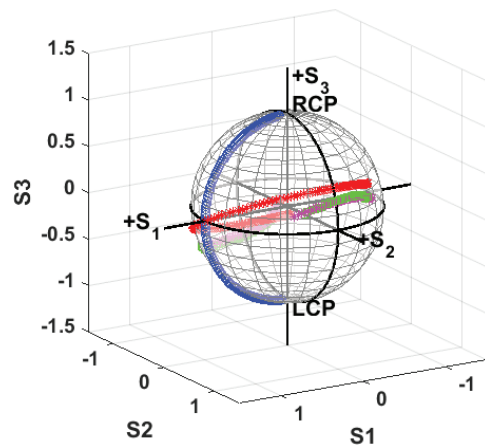


Figure 9: Poincaré sphere representation of SR beam polarization. Red=model, green=measured, magenta=measured phase shift, blue=SR source.

### ACKNOWLEDGMENTS

The authors would like to thank the China Scholarship Council, D.Van Campen and SPEAR3 staff for support of this work.

### REFERENCES

- [1] A. Hofmann, "The Physics of Synchrotron Radiation", Cambridge University Press, (2004).
- [2] J.Stöhr, *et al.*, "Element specific magnetic microscopy with circularly polarized X-ray", Science, Vol. 259, p.658 (1993).
- [3] G.G.Stokes, "On the composition and resolution of streams of polarized light from different sources", Trans. Camb. Phil. Soc., Vol. IX, p.399 (1852).
- [4] E.Collett, "Polarized Light: Fundamentals and Applications", Marcel Dekker, Inc., NY,p.34-49 (1992).
- [5] J.Corbett, C.L.Li, *et al.*, "Characterization of Visible SR at SPEAR3", IPAC15, Richmond, VA (2015).
- [6] C.L.Li, J.Corbett, J., T.Mistubishi, "Characterization of the visible beam polarization state at SPEAR3", IBIC2015, Melbourne, Australia (2015).
- [7] C.Limborg, *et al.*, "An Ultraviolet Light Monitor for SPEAR3", EPAC02, Paris, France (2002).
- [8] D.P.Arndt, *et al.*, "Multiple determination of the optical constants of thin film coating materials", Applied Optics, 23, No. 20, p.3594, (1984).
- [9] E.Hecht, *Optics*, 2<sup>nd</sup> Edition, Addison-Wesley (1987).
- [10] C.L.Li *et al.*, "Investigation of Continuous Scan Methods for Rapid Data Acquisition", IPAC15, Richmond, VA (2015).
- [11] C.L.Li, *et al.*, "Continuous scan capability at SSRL and application to X-ray diffraction", J. Synchrotron Radiation 23, p.912 (2016).